THE STRUCTURAL DESIGN OF TALL AND SPECIAL BUILDINGS
Struct. Design Tall Spec. Build. **19**, 421–438 (2010)
Published online 11 March 2010 in Wiley Interscience (www.interscience.wiley.com). **DOI**: 10.1002/tal.593

COLLAPSE RISK OF TALL STEEL MOMENT FRAME BUILDINGS WITH VISCOUS DAMPERS SUBJECTED TO LARGE EARTHQUAKES

PART I: DAMPER LIMIT STATES AND FAILURE MODES OF 10-STOREY ARCHETYPES

H. KIT MIYAMOTO[1,2], AMIR S. J. GILANI[2]*, AKIRA WADA[1] AND CHRISTOPHER ARIYARATANA[3]
[1] *Tokyo Institute of Technology, Ookayama, Meguro-ku, Tokyo, Japan*
[2] *Miyamoto International, West Sacramento, CA 95691, USA*
[3] *Arup Corporation, Formerly University of Illinois at Urbana-Champaign, Edison, NJ, U.S.A.*

SUMMARY

The design approach for tall steel moment frame structures with viscous dampers entails sizing steel members per code-level strength forces, and sizing viscous dampers to limit storey drifts. This method has been used extensively in new and retrofit applications. This methodology has resulted in structures that have longer periods than those using the code-designed approach, are economically competitive and have excellent performance in design-level earthquakes. However, the efficacy of this design in extreme events is not well understood because of the lack of limit states data for dampers and the absence of a field or analytical database of such structures subjected to large earthquakes. Mathematical modelling of viscous dampers with limit states was developed, correlated with experimental results and then used to analyse 10-storey archetypes. This analysis showed that the design had satisfactory performance during extreme seismic events. There were significant improvements in reducing collapse hazard by using an enhanced damper design with an increased damper safety factor. Copyright © 2010 John Wiley & Sons, Ltd.

1. INTRODUCTION

The seismic performance of tall steel special moment-resisting frames with fluid viscous dampers (hereinafter referred to as 'SMRF-FVD') subjected to large earthquakes was investigated. Using this structural system, steel members are designed for strength-level code forces, and the dampers are sized to control code limit drifts. In practice, FVDs are modelled—using the Maxwell representation—as a viscous dashpot element in series, with an elastic spring representing the driver brace used to connect the FVD to the structural members. Hence, the limit states of FVDs are not accounted for.

While satisfactory for design-level analysis, such modelling will not accurately represent the response of the damper when subjected to very large earthquakes because the damper limit states are not considered Thus, when performing near-collapse analysis, an FVD mathematical model that incorporates limit states must be used. Furthermore, the SMRF-FVD systems have not been subjected to large earthquakes. Therefore, the system performance at near collapse is not known. In addition, the influence that safety factors of the damper components have on the response has not been inves-

*Correspondence to: Amir S. J. Gilani, Miyamoto International, 1450 Halyard Drive, West Sacramento, CA 95691, USA. E-mail: agilani@miyamotointernational.com

Copyright © 2010 John Wiley & Sons, Ltd.

Table 1. Low- and mid-rise archetypes (Miyamoto *et al*., 2009b)

Archetype	O1	O2	O3	O4	A1	A2	A3	A4	B1	B2
Storeys	1	1	1	1	2	2	2	2	5	5
Column base	Pinned	Pinned	Fixed	Fixed	Pinned	Pinned	Fixed	Fixed	Fixed	Fixed
Design drift (%)	2·5	1·0	2·5	1·0	2·5	1·0	2·5	1·0	2·0	1·0
Damper FS	1·0	1·3	1·0	1·3	1·0	1·3	1·0	1·3	1·0	1·3
$Pr_{ColMCE\ (\%)}$	5·1	2·0	0·3	0·1	9·1	2·1	6·3	2·8	7·7	1·8
FEMA P695	Pass	Pass	Pass	Pass	Pass	Pass	Pass	Pass	Pass	Pass

FS is the factor of safety.
$Pr_{ColMCE\ (\%)}$ is the probability of collapse at the MCE level with a total system uncertainty (β) of 0·55.

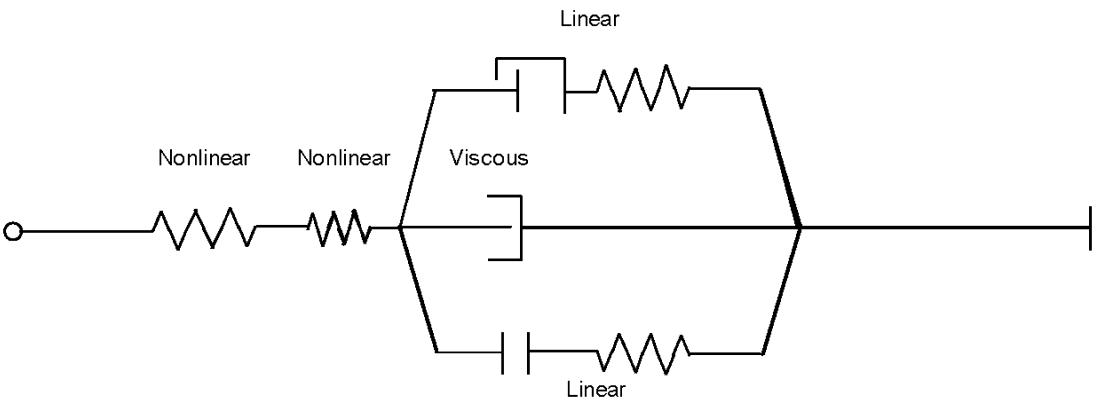

Figure 1. Block diagram for viscous dampers

tigated previously. To address these issues, incremental dynamic analysis (IDA) of a group of archetypes consisting of tall SMRF-FVD models, incorporating damper limit states, was performed.

The analysis used a damper model developed by the authors that incorporates limit states. The analysis and evaluation followed the techniques developed as part of the FEMA P695 (NEHRP, 2009) studies. Such an approach has been applied to a variety of building framings (Haselton and Deierlein, 2007). The primary objectives of the current study were to establish the probability of collapse at the maximum considered earthquake (MCE) intensity, and to assess the performance of tall steel SMRF-FVD buildings subjected to large earthquakes.

Recently completed studies (Miyamoto *et al*., 2009b) have shown the excellent performance of low- to mid-rise structures using SMRF-FVD when subjected to extreme earthquakes. For reference, the archetypes and evaluation data studied in this paper are listed in Table 1.

2. MATHEMATICAL MODEL OF VISCOUS DAMPERS WITH LIMIT STATES

2.1 Overview

A mathematical representation of FVDs incorporating the damper limit states has been developed by the authors (Miyamoto *et al*., 2009a) and was used for the studies (see Figure 1). This model consists of the driver brace, piston, piston undercut, viscous component and cylinder walls. Each element of the damper has a limit state. The elements not depicted in the figure were assumed not to control the limit state response.

Copyright © 2010 John Wiley & Sons, Ltd.

DOI: 10.1002/tal

2.2 *Damper limit states*

When the FVD displacement is less than the design stroke, it acts as a viscous damping element (dashpot) consistent with the Maxwell representation. However, when this limit is exceeded, contact between the metal parts at the ends of the damper produces axial force in the cylinder wall. To account for this phenomenon, gap and hook elements with openings equal to the available spacing and with stiffness equal to that of the cylinder wall are included in the model.

The piston undercut, approximately 13 mm (0·5 in.) long, is the machined-down (reduced area) section of the piston rod between its smooth surface and the threaded portion of the rod. In compression, the piston undercut yields without buckling because of its short length. In tension, yielding of the piston undercut is followed by tensile fracture, rendering the damper useless.

The driver brace—used to attach the damper to the SMRF members—is designed for both strength and stiffness. The brace must have sufficient compressive and tensile capacity to withstand the axial load delivered by the damper at the MCE level. Additionally, the driver must have sufficient stiffness to activate the viscous element. When the brace buckles, the damper is rendered ineffective.

2.3 *Nonlinear response with limit states activation*

Sinusoidal loading of increasing amplitude was applied to the damper model of Figure 1 to verify the limit states of the model. Sample simulation data are shown in Figure 2. At 4·5 s in the response, the piston extension reached the stroke limit, the damper bottomed out and the damper was converted to a stiff elastic brace. Next, the piston undercut yielded, but it did not fracture. Loading was then reversed. This resulted in disengagement of the cylinder walls and reloading of the viscous component. At 5·3 s, the piston bottomed out again. Loading was increased further, resulting in tensile yielding and the subsequent fracture of the piston undercut. The FVD was then ineffective, and was thus removed from the model.

2.4 *Experimental verification*

Experimental data (Taylor Devices, personal communication, 2009) were used to assess the accuracy of the FVD model of Figure 1. This damper was subjected to large pulses during laboratory tests, and

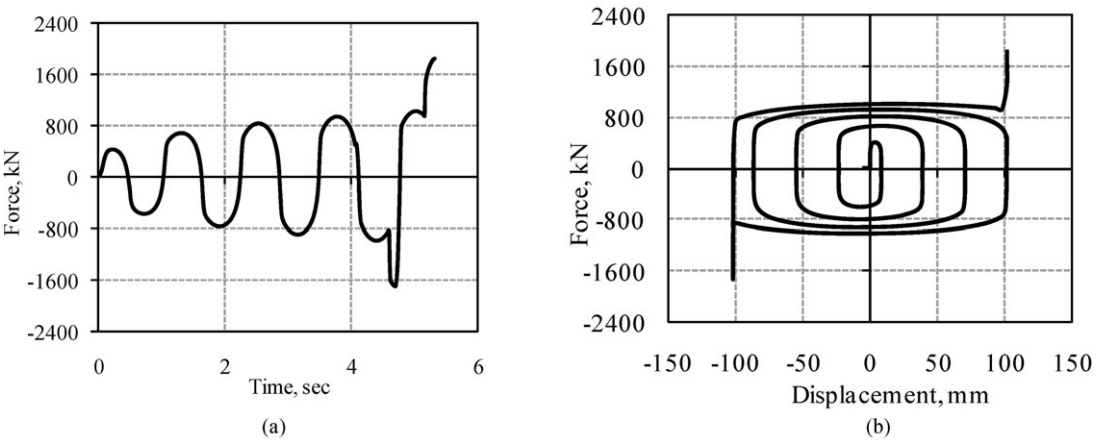

Figure 2. Response of an FVD incorporating stroke and force limit states. (a) FVD force history. (b) FVD force–displacement hysteresis

Copyright © 2010 John Wiley & Sons, Ltd.

DOI: 10.1002/tal

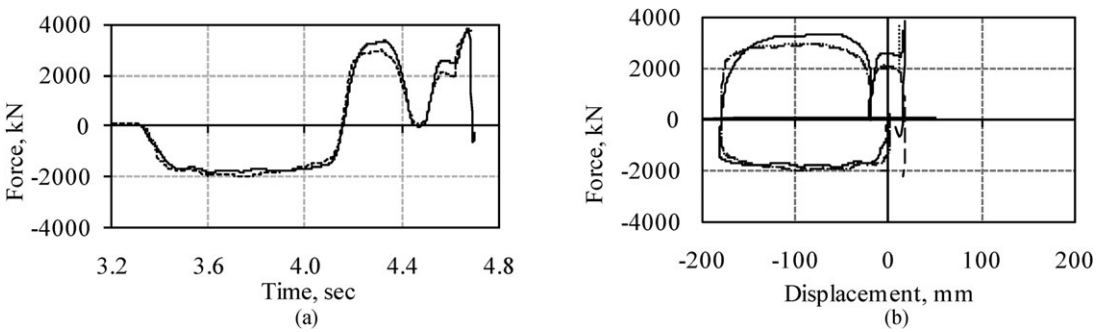

Figure 3. Experimental (solid line) investigation of damper limit states and analytical (dashed line) correlations. (a) Force response. (b) Force–displacement hysteresis

reached its limit states. The damper had the constitutive relation of Equation (1) (kN and mm units), a nominal capacity of 2000 kN (450 kips) and a stroke of 130 mm (5·125 in.). To capture its limit states, the piston was extended to within 3 mm (0·125 in.) of its available stroke in tension.

$$F = 195\,\mathrm{sgn}(v)|v|^{0.4} \tag{1}$$

The experimental responses are shown as solid lines in Figure 3. The analytical responses are shown as the dashed lines in the figure. The following FVD limit states can be identified in this figure: at 4·3 s, the FVD was pulled in tension at 910 mm/s (36 in./s), and the motion was reversed just before the damper bottomed out. This large velocity was close to 300% of the damper's nominal design value. At this velocity, the internal pressure increased and the cylinder wall expanded, which limited the increase of the damper force. At 4·6 s, the damper bottomed out in tension, thus activating the cylinder wall. This was followed by tensile yielding and fracture of the piston undercut at 4·7 s. The dashed lines in Figure 3 represent the results obtained from analysis. Good correlation was obtained between the experimental data and the analytical simulations.

2.5 Comparison of the responses with the damper model without limit states

To assess the influence of limit state on responses, a damper was subjected to further analysis. The subject damper had the constitutive relation of Equation (2) (kN and mm units), a nominal capacity of 670 kN (150 kips) and a stroke of 100 mm (4 in.):

$$F = 30\,\mathrm{sgn}(v)|v|^{0.3} \tag{2}$$

Analysis was conducted for both the damper model with limit states (Figure 1) and the simple dashpot damper model without limit states. The two analytical models were subjected to the Kobe/NIS000 (PEER, 2009a) record using intensities of 100, 125 and 175% of nominal. The results are presented in Figure 4 and the following:

(1) At 100% intensity, the only force in the damper unit is the viscous component. At this level, the force in the cylinder wall is zero, and the two models produce the same hysteresis response.
(2) At 125% intensity, the damper bottoms out during analysis, and significant force develops in the cylinder walls for the damper with limit states. The magnitude of this force is much larger than that in the dashpot element. The two components can also be out of phase, resulting in a net force

Copyright © 2010 John Wiley & Sons, Ltd.

DOI: 10.1002/tal

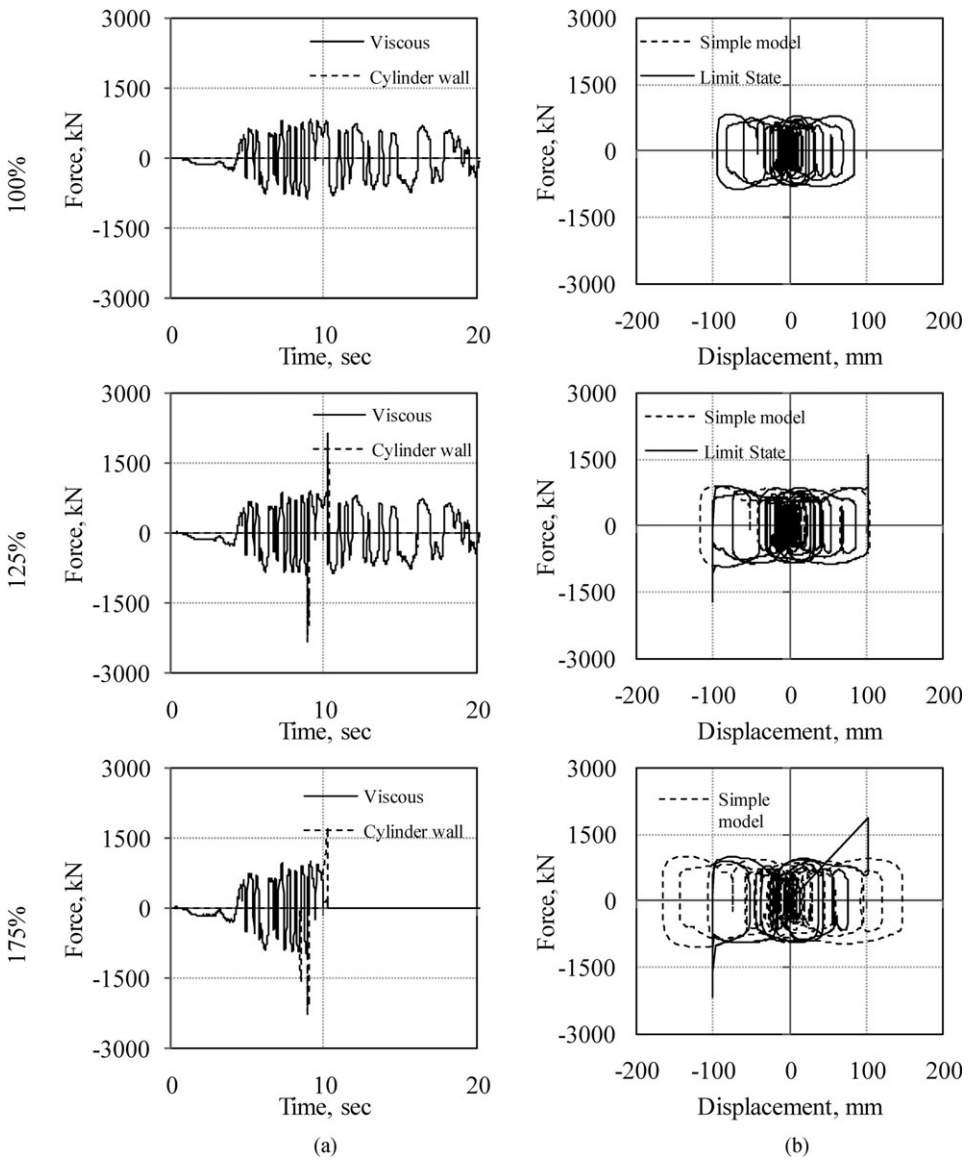

Figure 4. Response of the limit state and Maxwell models, Kobe record. (a) Components of damper force. (b) Damper hysteresis

that is smaller than the one present in the cylinder wall. The damper without limit states will significantly underestimate the force that is delivered to damper connections and structural frames. This simple model also overestimates the energy dissipated by the system.

(3) At the 175% intensity, the damper with limit states bottoms out during analysis, and significant force develops in the cylinder walls. Next, the piston undercut fractures, rendering the damper ineffective. The damper without limit states will significantly underestimate the force that is delivered to the damper connections and assembly. In this case, the energy dissipation capacity

Copyright © 2010 John Wiley & Sons, Ltd.

DOI: 10.1002/tal

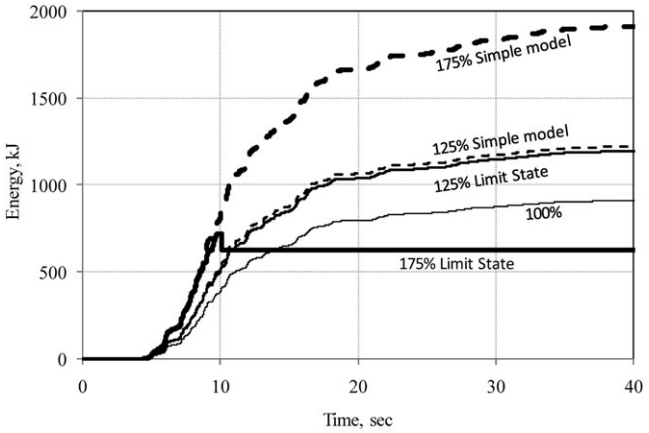

Figure 5. Dissipated energy responses, Kobe record

Table 2. Damper force and dissipated energy

	Damper force (kN)			Dissipated energy (kJ)		
Intensity (%)	100	125	175	100	125	175
Damper with limit states	880	2400	2400	920	1200	720
Damper without limit states	880	950	1050	920	1230	1920
Error (%)	0	–60	–56	0	2	166

of the damper is exaggerated. This can lead to overstress in the steel moment frame components because the damping present in the system is overestimated.

Figure 5 presents the dissipated energy by the damper from the analysis described here. When the damper reaches a limit state, the damper model without limit states is not able to accurately track the physical response of the damper. After the piston undercut fails, the damper is ineffective. However, the simple model continues to presume that the unit can still effectively dissipate the seismic input energy as shown in Figure 5.

Table 2 summarizes the analytically computed force in the damper element and the energy dissipated by the viscous damper component for the two models at the three intensity levels. As listed in the table, when the damper bottoms out, the elements in line with the damper will experience forces that are 60% larger than those predicted by the simple damper model without limit states. Similarly, the damping delivered to the system and the ability of the damper to dissipate the seismic energy are overestimated by more than 100% after the piston undercut fractures.

3. ANALYSIS AND EVALUATION METHODOLOGY

3.1 Design procedure

3.1.1 Overview

The archetypes used in this study were designed based on the code provisions (ASCE, 2005). Member sizes were determined by the strength provisions without regard for lateral drift limitations. The FVDs were then sized to limit the storey drift ratios.

Copyright © 2010 John Wiley & Sons, Ltd.

DOI: 10.1002/tal

3.1.2 Seismic loading

The seismic demand was based on a typical location in the Los Angeles area (importance factor of 1·0, site class D), with mapped short-period (S_s) and 1 s (S_1) spectral accelerations of 1·5 and 0·6 g, respectively. These values are consistent with the maximum hazard values used in FEMA P695 (NEHRP, 2009). Also consistent with FEMA P695, the maximum allowable period as defined in ASCE/SEI 7–05 (ASCE, 2005) was used in collapse evaluation.

3.1.3 Design of moment frame members

The provisions of the AISC Load and Resistance Factor Design (AISC, 2005a) were used to size the members of the steel SMRFs. The design was based on the equivalent lateral force procedure of ASCE/SEI 7–05. The redundancy factor (ρ) equalled 1·0 for all archetypes. The code-allowed reduction of design forces to 75% was not considered because the FVDs were not added to all the floors. The requirements of the AISC seismic provisions (AISC, 2005b) for SMRFs were implemented in the design. Reduced beam sections (RBSs), classified as a prequalified connection (AISC, 2005c) for seismic applications were assumed in modelling. Typical to design practice, single column and beam sections per floor were used, and column splices were provided at every third floor.

3.1.4 Design of dampers

After the moment frames were designed per code, FVDs were then sized to limit storey drift ratios to the values permitted by code. Because the dampers had a velocity coefficient (α) of 0·5 and not all the floors in a typical model were damped, neither the linear static nor the linear dynamic procedure outlined in the code was used. Instead, a nonlinear response history analysis was used. Three spectrum-matched records were developed; see Figure 6. The damper constant C was then chosen to limit the storey drifts from the maximum responses of these analyses to the code-prescribed values or the enhanced performance targets at the design earthquake (DE) intensity. The maximum FVD responses at the MCE level with applicable safety factors were then supplied to damper manufacturers for damper design (Taylor Devices, personal communication, 2009). For some archetypes, the code minimum safety factor of 1·0 at MCE with storey drift ratios of 2% was used. For other archetypes, enhanced performance (Miyamoto and Gilani, 2008) was chosen, using a safety factor of 1·3 at MCE, with storey drift ratios limited to 1%.

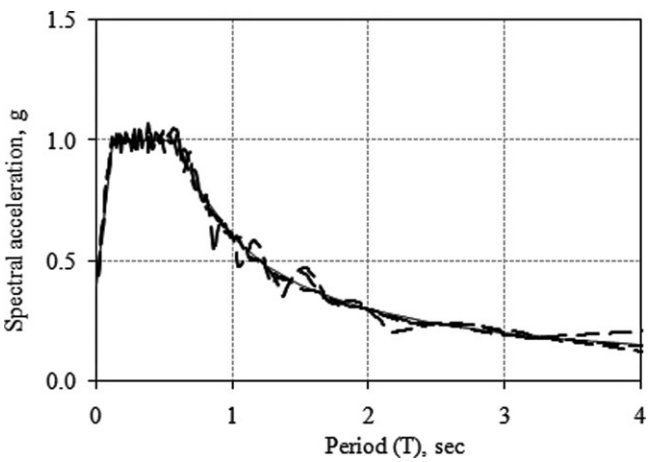

Figure 6. DE spectrum (solid line) and response spectra from spectrum-matched records (dashed lines)

Copyright © 2010 John Wiley & Sons, Ltd.

DOI: 10.1002/tal

3.2 Analysis procedure

3.2.1 Overview

The program OpenSees (PEER, 2009b) was used to conduct nonlinear analysis. Models used linear beams with concentrated plastic hinges to represent RBSs, nonlinear beam–column elements and the model of Figure 1 for FVDs. For the SMRF columns, the procedure described in ASCE/SEI 41–06 (ASCE, 2006) was used to determine the nonlinear moment–rotation relations. The moment–rotation behaviour for the RBS rotational spring was derived from the modelling parameters developed by Lignos and Krawinkler (2007). The models were preloaded with concentrated gravity loads prior to seismic analysis. Lumped mass representation was used for the models, and inherent damping was assumed to be mass and stiffness proportional, and equivalent to 2% of critical.

3.2.2 Input histories

The input histories used in analysis were based on the two components of the 22 far-field Next Generation Attenuation (PEER, 2009a) records. These records have been identified by FEMA P695 for collapse evaluation analysis. These records correspond to a large sample of strong recorded motions that are consistent with the code, and are structure and site hazard independent. Figure 7 presents the acceleration response spectra for these records. The MCE spectrum is shown as the solid line in the figure. For analysis, the 44 records were normalized to remove the record-to-record variation in intensity (NEHRP, 2009).

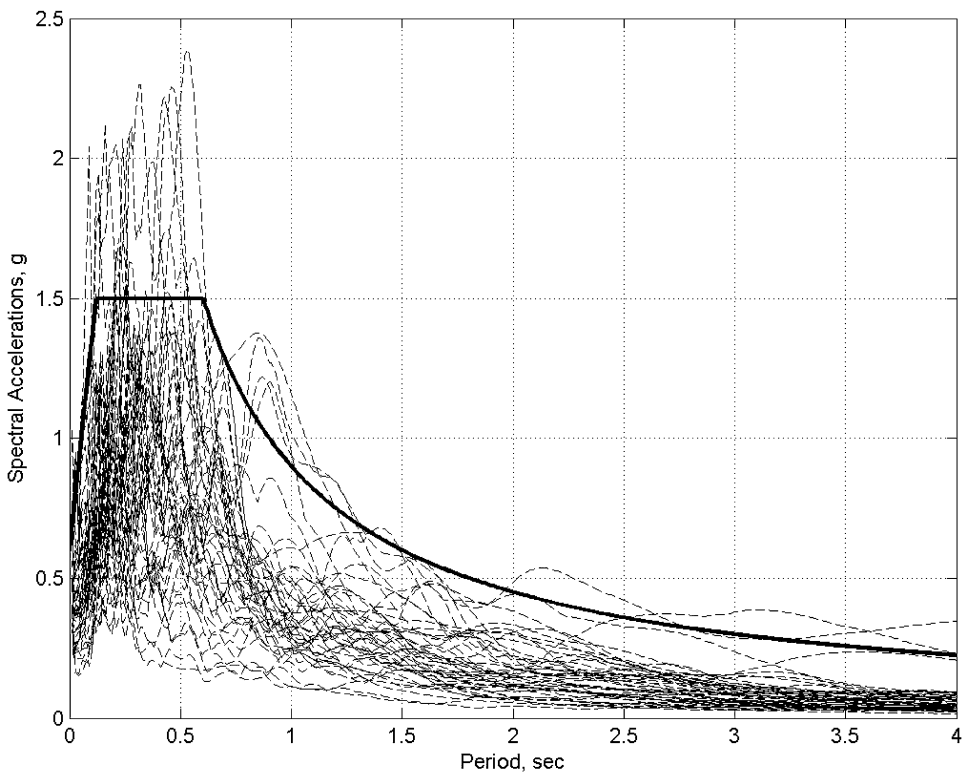

Figure 7. Response spectra for the NGA records and the MCE spectrum (solid line)

Copyright © 2010 John Wiley & Sons, Ltd.

DOI: 10.1002/tal

3.3 Analysis programme and evaluation procedure

3.3.1 Pushover analysis

Nonlinear static (pushover) analysis of the models was conducted to compute the system ductility. This procedure was used to compute the spectral shape factor (*SSF*) for collapse probability calculations. The *SSF* modification is required to correct the spectral shape of the records for very large earthquakes, because their frequency content differs from those of earthquakes with lesser intensities. Since viscous dampers are velocity-dependent components, they were not activated in static analysis as long as the limit states were not reached. The pushover analyses resulted in nonlinear force–displacement relations. Bilinear curves were then fitted to the computed pushover curves to compute the yield (δy) and ultimate (δu) roof displacements or drifts. The computation of the *SSF* is based on the following equations from FEMA P695:

$$\mu^*_c = \min\left(\mu c = \frac{\delta u}{\delta y}, 8{\cdot}0\right) \tag{3}$$

$$SSF = e^{0{\cdot}17(\mu^*_c - 1)^{0{\cdot}33}(1{\cdot}5 - 0{\cdot}6(1{\cdot}5 - T_{\max}))} \tag{4}$$

3.3.2 IDA

IDA simulation (Vamvatsikos and Cornell, 2005) is a powerful tool used to determine the collapse response of structures. Of interest for this study was the computed IDA plot of the maximum floor drift versus input spectral intensity. For collapse analysis, the normalized records were scaled and applied to the models to obtain sufficient data points to determine the nonlinear response up to collapse. In this paper, collapse is defined as the lesser of the following, and is consistent with the value used by other researchers (Haselton and Deierlein, 2007): a drift ratio of 18%, or drift at a point at which the tangent stiffness is reduced to 5% of the initial elastic stiffness. After the IDA was completed for an archetype, the collapse spectral intensity (S_a) for the 44 records was tabulated, and the median of the collapse data, denoted as the median collapse capacity (S_{CT}), was determined. The MCE spectral acceleration at T_{max} was designated as S_{MT}. The collapse margin ratio (*CMR*) was then computed from the following:

$$CMR = \frac{S_{CT}}{S_{MT}} \tag{5}$$

The adjusted collapse margin ratio (*ACMR*) was computed to adjust the *CMR* for the *SSF*:

$$ACMR = SSF * CMR \tag{6}$$

3.3.3 Fragility curve (probability of collapse at MCE)

The 44 collapse points obtained from the IDA of a response quantity were treated as a random variable with log-normal distribution and were statistically organized. A log-normal cumulative distribution function (CDF) was fitted to the data to obtain the theoretical mean, median and standard deviation of the data. The following two modifications were then made, and the ordinate of the modified plot at the MCE intensity presents the probability of collapse at that intensity:

(1) The CDF was modified to have a system collapse uncertainty (β_{tot}) of 0·55, consistent with the FEMA P695 value for superior ('A') quality of both the test data and the model. The result was a rotation in the CDF around the median point.
(2) The CDF was then modified to account for the *SSF*, which resulted in a shift in the CDF.

Copyright © 2010 John Wiley & Sons, Ltd.

DOI: 10.1002/tal

For structures with FVDs, of particular interest is the intensity when the damper bottoms out (stroke limit) or fails (force limit). Fragility plots of these quantities for the dampers provide important information on the adequacy of the damper properties and the effect of the damper factor of safety on the response. These damper fragility plots were processed with a β_{tot} of 0·55, but without the *SSF* modification. Such an approach is conservative.

4. ARCHETYPES

4.1 Analysis matrix

The seismic performance of a tall steel SMRF-FVD structural system was investigated by considering the behaviour of five tall (10-, 20- and 30-storey) archetypes. As part of this investigation, a 40-storey archetype was also prepared. However, this structure had a period of approximately 6·1 s, and typically available acceleration records are not reliable at such high periods due to the limits on their frequency content. Preliminary analysis showed that the responses for the 40-storey archetype were underestimated from response history analyses using the available records. Therefore, this archetype was not pursued further.

The two damper configuration safety factor conditions and performance targets for the 10- to 30-storey archetypes were evaluated. Table 3 presents the archetype matrix used in analysis. The results from the first two archetypes are presented here. A companion paper being prepared will present a detailed discussion of results for the 20- and 30-storey archetypes.

4.2 Archetype geometry

The first floor and typical storeys were 13 ft tall, and typical bays were 30 ft wide. The archetypes were square in plan and comprised five bays in each direction. The SMRFs were provided along only the perimeter (as is the typical US industry practice). Two-dimensional modelling along one of the principal directions was used to characterize the response of the structures. The 10-storey models had three bays of moment frames.

Figure 8 presents the elevation view of the 10-storey archetypes. Each model represents an exterior framing in the east–west direction. One more gravity bay was placed on each side of the archetypes to account for the combined stiffness of all interior gravity columns, resulting in the seven bays shown in the figure. Each super-column had a stiffness that was four times the nominal interior column stiff-

Table 3. List of archetypes used in analysis of tall buildings

Archetype	Configuration			Design values			Dampers	
				Period (s)		Design drift		
ID	Storeys	Column base	Mass (mg)	T_n	T_{max}	(%)	FS	NDF
C1	10	Fixed	4 500	2·96	1·93	2·0	1·0	5
C2	10	Fixed	4 500	2·96	1·93	1·0	1·3	9
D1	20	Fixed	9 100	3·57	3·35	2·0	1·0	13
D2	20	Fixed	9 100	3·57	3·35	1·0	1·3	19
E1	30	Fixed	13 000	5·01	4·64	1·0	1·0	19

T_{max} denotes the maximum allowable period by ASCE/SEI 7–05.
T_n denotes the fundamental period obtained from dynamic analysis.
FS is the factor of safety.
NDF is the number of damped floors.

Copyright © 2010 John Wiley & Sons, Ltd.

DOI: 10.1002/tal

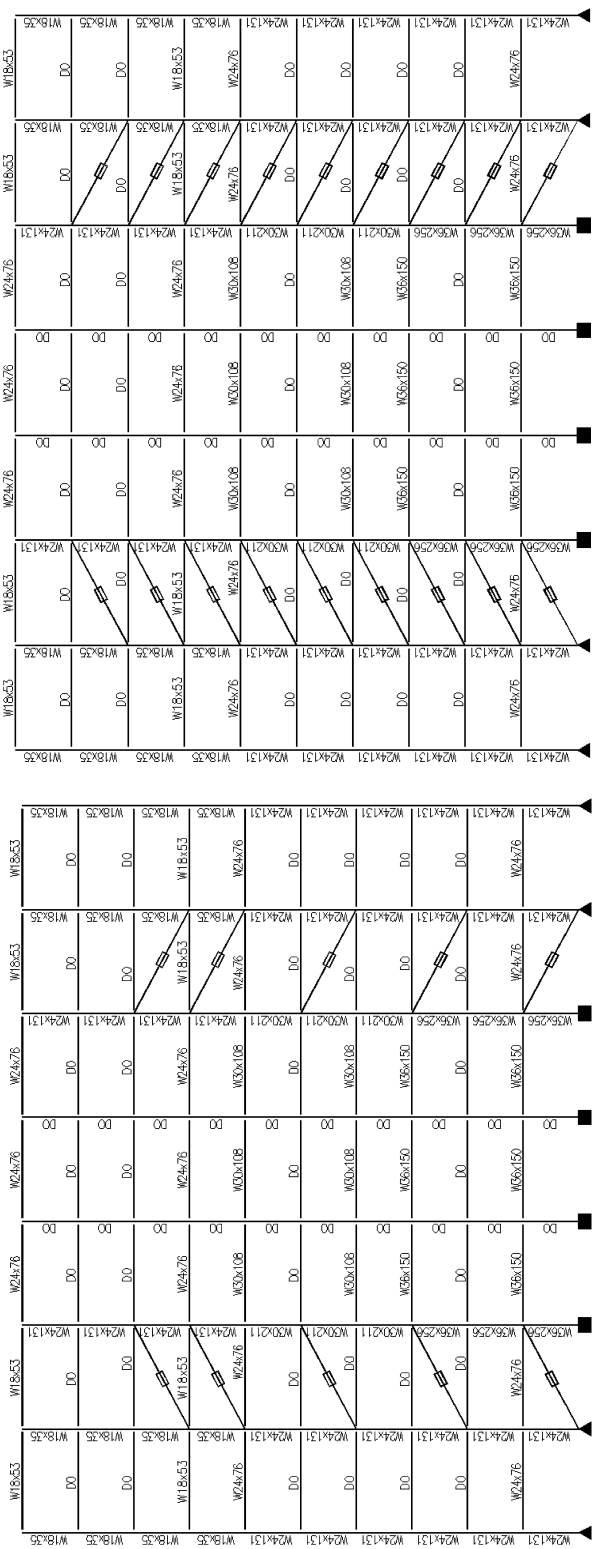

Figure 8. Elevation views of the 10-storey archetypes: (a) C1 and (b) C2

Copyright © 2010 John Wiley & Sons, Ltd.

DOI: 10.1002/tal

ness. The super-columns were included in the model to assess realistically the collapse performance of the building after the dampers and the SMRFs had reached their limit states.

4.3 Viscous damper selection

For each archetype, limited damper sizes were used throughout the building height. Because the computed storey drift was similar for most floors, it was economical to use limited damper sizes. Several iterations were used to select the location of the damped floors. The selected configurations provided an effective solution to limit storey drift. The storey drift at the first floor was less than at the floors above for the design load because the bases of the columns were fixed. However, as is common in design practice, dampers were included in these floors to provide vertical continuity.

5. ANALYSIS RESULTS

5.1 Pushover analysis

Figure 9 presents the pushover curves for archetypes C1 and C2 as solid lines. A typical pushover curve consists of an elastic portion followed by structural yielding. This, in turn, is followed by significant stiffening as the dampers bottom out and are converted to steel braces. The stiffening is significantly larger for the C2 archetype because the dampers have higher capacity in this model. Next, as dampers fracture in tension or buckle in compression, the stiffness drops sharply. Finally, the structure itself reaches its limit state.

Also shown in the same figure is the pushover curve for the case when no dampers were used in analysis as dashed line. The effect of including dampers in analysis is shown by the difference in the two plots. Because the archetypes have several dampers, the descending slope of the damper failure comprises several segments, each corresponding to the failure of different dampers C2 has higher capacity than C1 does, and the two cases have similar ductility because the moment frames have identical sections. The procedure described in FEMA P695 is used to fit a bilinear curve to the data (dotted line in the figures), and to compute the yield and ultimate points (identified as points in

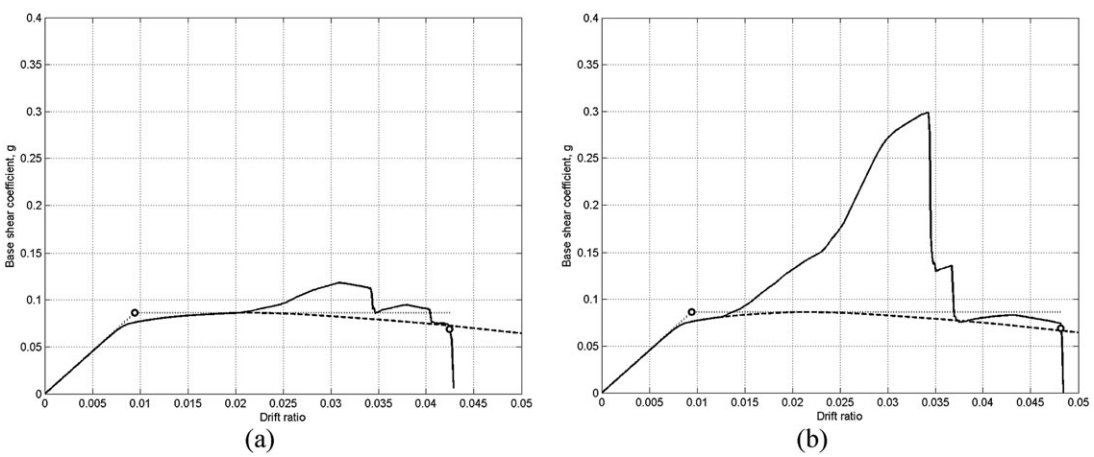

Figure 9. Pushover curves for the models, SMRF without damper (dashed line), SMRF-FVD (solid line) and bilinear approximation (dotted line): (a) C1 and (b) C2

Copyright © 2010 John Wiley & Sons, Ltd.

DOI: 10.1002/tal

the figures). The computation for the *SSF* is then based on the system ductility, and is presented in Table 4.

5.2 *IDA results*

Figure 10 presents the IDA plots for the archetypes C1 and C2. For a majority of the analysis cases, the collapse performance was governed by the drift limitation of 18%. The thick solid and the thick dashed horizontal lines in Figure 10 denote the S_{MT} and S_{CT} spectral intensities, respectively. Table 5 presents the *ACMR* for the archetypes. FEMA P695 specifies a minimum acceptable *CMR* of 1·59. Both archetypes have *ACMR*s that are greater than 1·59, so the collapse safety margin for both archetypes is acceptable. These results indicate that for the 10-storey structures, the SMRF-FVD system is dependable, with a large margin against collapse at the MCE intensity. It is further noted that adding

Table 4. Archetype pushover analysis results

Archetype	u_y	u_{max}	μ^*_c	*SSF*
C1	0·0095	0·043	4·5	1·46
C2	0·0095	0·048	5·1	1·50

u_y and u_{max} are the yield and ultimate drifts.
μ^*_c is the system ductility.

Table 5. Archetype IDA results

Archetype	S_{CT} (g)	S_{MT} (g)	*CMR*	*ACMR*
C1	0·77	0·47	1·65	2·43
C2	0·98	0·47	2·09	3·14

S_{CT} is the median spectral acceleration at collapse.
S_{MT} is the MCE spectral acceleration.

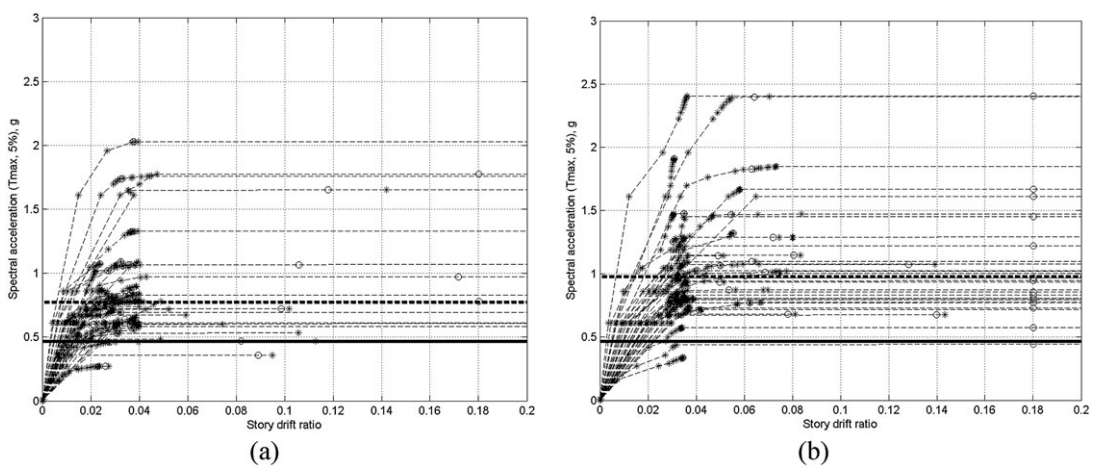

Figure 10. IDA plots for the models (solid and dashed thick lines indicate the MCE and median collapse intensities, respectively): (a) C1 and (b) C2

Copyright © 2010 John Wiley & Sons, Ltd.

DOI: 10.1002/tal

a relatively small (1·3) factor of safety to the damper stroke and force capacities increases the *ACMR*s significantly, from 2·4 to 3·1, or an increase of 29%.

5.3 Collapse mechanism

Table 6 presents the percentage of collapsed floors for the two archetypes. For C2, all the collapse modes corresponded to a single-storey mechanism. For C1, a few two-storey collapse mechanisms were observed at the upper floors. Also for C1, nearly half of the collapses occurred on the fourth floor, and only 20% of the collapses involved the bottom three storeys. For C2, 74% of the collapses occurred at the bottom three floors, with 36% of the collapses at the first floor.

For archetype C1, the fourth floor had no damper and also had a reduced column size. This combination contributed to the large collapse probability at this level. For archetype C2, although the bottom floor dampers had a factor of safety of 1·3, they were designed for a drift ratio of 1·0% and thus had a small stroke capacity. At the DE, these floors had storey drift ratios of 0·9% to approximately 1·0%. Therefore, the damper at these floors bottomed out and then failed prior to the upper-level dampers reaching their stroke limits. Such a failure mode can be mitigated by specifying larger damper factors of safety for the stroke at the bottom storey of structures.

Figure 11 presents the median storey shear distribution for the two archetypes at DE, MCE and collapse intensities. For each level and intensity, the shown values correspond to the computed median

Table 6. Archetype collapse analysis

	Floor										
Archetype	10th (%)	9th (%)	8th (%)	7th (%)	6th (%)	5th (%)	4th (%)	3rd (%)	2nd (%)	1st (%)	Sum (%)
C1	19	2	**2**	**2**	2	**7**	46	**9**	–	**11**	100
C2	5	–	–	–	–	**7**	**14**	**11**	**27**	**36**	100

For both archetypes, the bold entries correspond to the floors with dampers.

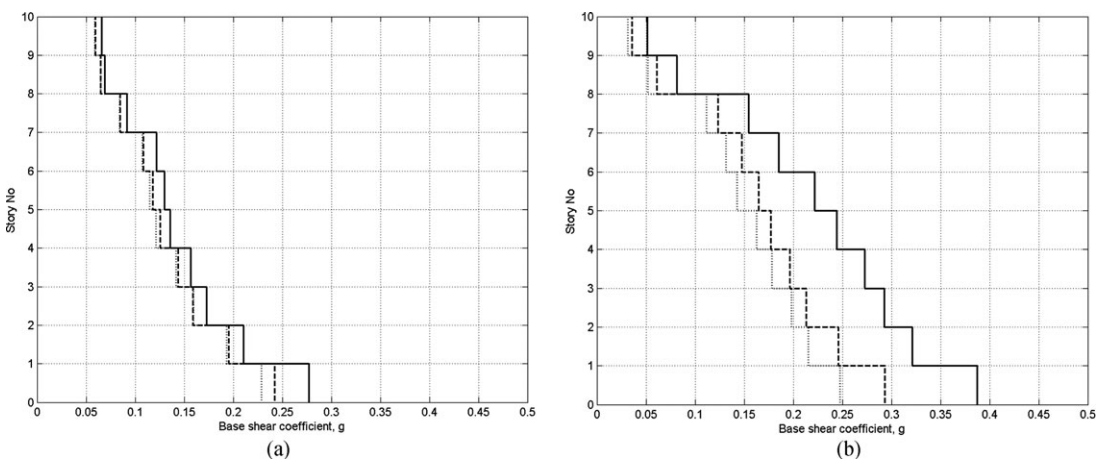

Figure 11. Median storey shear distribution at DE (dotted line), MCE (dashed line) and collapse (solid line): (a) C1 and (b) C2

Copyright © 2010 John Wiley & Sons, Ltd.

DOI: 10.1002/tal

of the responses from the 44 records. For archetype C2, the storey shear at collapse was significantly larger than at the MCE level, which contributed to the large number of bottom floor collapses. This pattern was not observed for archetype C1.

5.4 Fragility analysis

Figure 12 presents the system fragility plots for the archetypes. As noted earlier, the test data and curve were fitted and then adjusted (rotated and shifted) to account for system uncertainty and the *SSF* effect. The probabilities of failure at the MCE intensity, obtained from these plots, are listed in Table 7. For the archetypes, this probability was significantly less than the 20% that FEMA P695 specifies as the limiting value of acceptable performance for the structural systems.

As shown in Figure 12 and Table 7, adding the 1·3 factor of safety to the damper components resulted in an approximately threefold reduction in collapse probability. Such an increase in damper size is cost-effective, and it would significantly improve the response of the tall damped steel SMRF-FVD structures when subjected to large earthquakes. Dampers with a sufficient factor of safety decrease the collapse probability to an insignificant number. It is therefore recommended that the collapse probability should be limited to a value less than the 20% limit per FEMA P695 for large, tall structures, because a greater number of lives are at stake in this type of structure.

5.5 Damper responses

Figure 13 presents the damper fragility plots for the stroke and force, respectively, for archetype C1. The shown plots are for the first damper that reached its limit state, and they do not necessarily cor-

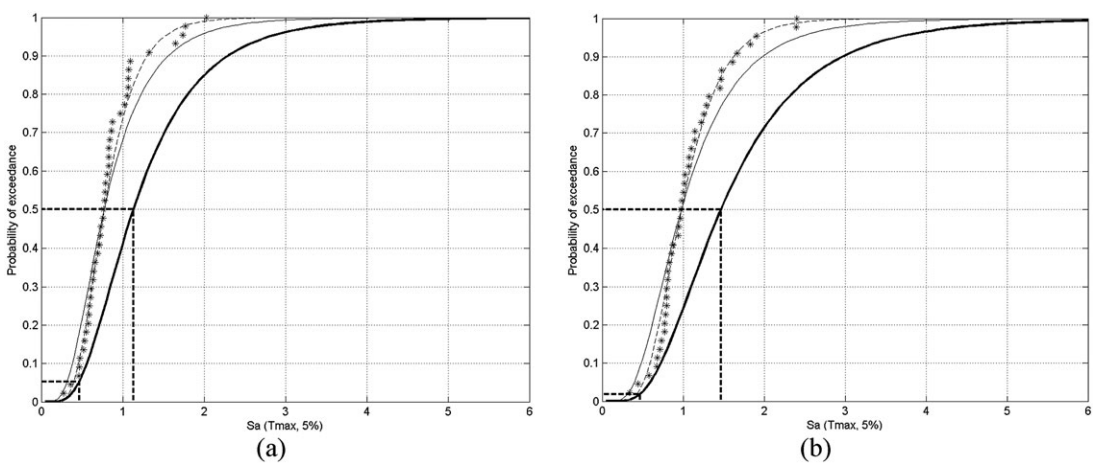

Figure 12. System fragility plots for archetypes: (a) C1 and (b) C2

Table 7. Archetype fragility analysis

Archetype	C1	C2
$Pr_{ColMCE\,(\%)}$	5·3	1·9

$Pr_{ColMCE\,(\%)}$ is the probability of collapse at the MCE level with a total system uncertainty (β) of 0·55.

Copyright © 2010 John Wiley & Sons, Ltd.

DOI: 10.1002/tal

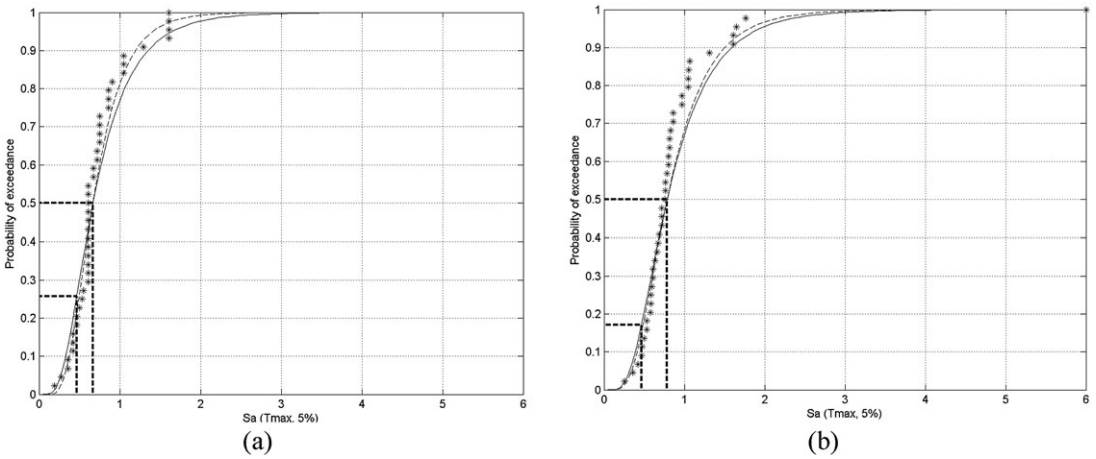

Figure 13. Damper fragility plots for archetype C1: (a) stroke and (b) force

Table 8. Damper fragility analysis

	S_a* (*g*)		Pr* (%)	
Archetype	Stroke	Force	Stroke	Force
C1	0·67	0·79	26	17
C2	0·74	0·97	20	9

S_a* is the median spectral intensity for the damper limit states.
Pr* denotes the probability of reaching the damper limit states at the given MCE intensity.

respond to a particular floor. Note that the probability of reaching the damper stroke and force limit states is approximately 26 and 18%, respectively, at the MCE intensity. Table 8 lists the median intensity for the dampers reaching the limit states and the probability of reaching limit states at the MCE intensity. It was noted that when a factor of safety larger than the code minimum was included in the damper design, the probability of reaching the stroke or the force limit state at the MCE-level intensity was reduced significantly. It is therefore important to use a high safety factor and quality dampers for reliable performance.

5.6 System performance

Table 9 summarizes the performance of the two 10-storey archetype indexes and the system of the archetypes. It should be noted that all the models and the system as a group meet the *ACMR* and the collapse probability requirements at the MCE level. Therefore, they are labelled as 'pass' given their acceptable performance. The archetypes have a very large margin of safety compared with acceptable thresholds. Thus, it can be expected that the 10-storey SMRF-FVDs using the code-recommended factor of safety (1·0) will perform adequately in large earthquakes. The collapse probability at the MCE level is significantly reduced if a nominal (1·3) factor of safety is included in design of the damper components.

Copyright © 2010 John Wiley & Sons, Ltd.

DOI: 10.1002/tal

Table 9. System performance

Archetype	Storeys	*ACMR*	Pr_{ColMCE} (%)	*ACMR*_Accept	Pr_{ColMCE}_Accept (%)	Check
C1	10	2·43	5·3	1·59	20	Pass
C2	10	3·14	2·1	1·59	20	Pass
System	10	3·04	3·7	2·02	10	Pass

6. FUTURE STUDIES

The analysis presented in this paper used mathematical modelling of viscous dampers, including damper limit states, to assess the performance of tall (10-storey) steel SMRF-FVD systems subjected to large earthquakes. A companion paper, currently under preparation, extends this study to taller SMRF-FVD buildings, and presents analytical results for 20- and 30-storey structures.

7. SUMMARY AND CONCLUSIONS

The IDA of steel SMRF-FVD archetypes was carried out to assess the probabilistic response of this design applied to 10-storey models in large earthquakes. A detailed model of the fluid viscous dampers, incorporating the damper limit states, was included in the archetypes evaluated. The archetypes were then subjected to pushover and incremental dynamic analyses, and the collapse margin and the collapse probability at the MCE intensity were determined. Based on the analytical results, the following conclusions were made:

(1) The mathematical model of dampers incorporating the damper limit states can be used to represent the physical properties of viscous dampers and the effect of these properties on structural response. This model correlates well with experimental data.
(2) When subjected to large earthquakes, a simple dashpot damper model without limit states will underestimate the force that develops in the dampers, and overestimate the energy dissipation in the damper. This combination could result in underestimating the demand on the damper connections and the steel moment frame elements.
(3) The SMRF-FVD 10-storey system, using the code minimum factor of safety, provides excellent performance at the MCE and large earthquake intensities. The system has a sufficient margin against collapse, and therefore has a probability of collapse at the MCE intensity that is far below the FEMA-recommended values.
(4) The SMRF-FVD system that uses both an enhanced design and a damper factor of safety of 1·3 has a significantly greater margin against collapse than the code-minimum SMRF-FVD system does. The probability of collapse at the MCE level is significantly decreased, and the level of protection provided in large earthquakes is increased.
(5) Dampers with a sufficient factor of safety decrease the collapse probability to an insignificant number. It is the authors' opinion that the collapse probability should be limited to much less than the 20% limit specified by FEMA for large, tall structures, because a larger number of lives are affected by this type of structure.
(6) The enhanced performance objective of 1% drift resulted in almost exclusive lower-storey collapse mechanisms. Further investigations are currently under way to determine the effect on the collapse modes of SMRF-FVD using a larger stroke factor of safety for the bottom-storey dampers.

Copyright © 2010 John Wiley & Sons, Ltd.

DOI: 10.1002/tal

ACKNOWLEDGEMENTS

The authors acknowledge financial support from Taylor Devices and Amour Steel. The technical assistance of Mr Doug Taylor and Mr John Metzger of Taylor Devices, and Mr Steve Ayers from Amour Steel is also acknowledged.

REFERENCES

AISC (American Institute of Steel Construction). 2005a. *ANSI/AISC 358–05: Prequalified Connections for Special and Intermediate Steel Moment Frames for Seismic Applications*. AISC: Chicago, IL.

AISC (American Institute of Steel Construction). 2005b. *AISC 341–05: Seismic Provisions for Structural Steel Buildings*. AISC: Chicago, IL.

AISC (American Institute of Steel Construction). 2005c. *AISC 360–05: Specification for Structural Steel Buildings*. AISC: Chicago, IL.

ASCE (American Society of Civil Engineers). 2005. *ASCE/SEI 7–05*: *Minimum Design Loads for Buildings and Other Structures*. ASCE: Reston, VA.

ASCE (American Society of Civil Engineers). 2006. *ASCE/SEI 41–06: Seismic Rehabilitation of Existing Buildings*. ASCE: Reston, VA.

Haselton CB, Deierlein GG. 2007. Assessing seismic collapse safety of modern reinforced concrete moment frame buildings. *John A. Blume Earthquake Engineering Center report no. TR-156*, Department of Civil and Environmental Engineering, Stanford University, Palo Alto, CA.

Lignos DG, Krawinkler H. 2007. A database in support of modeling of component deterioration for collapse prediction of steel frame structures. In *Proceedings of ASCE Structures Congress*, Structural Engineering Institute, Long Beach, CA, May 16–19, 2007.

Miyamoto HK, Gilani ASJ. 2008. Design of a new steel-framed building using ASCE 7 damper provisions. In *Proceedings of ASCE Structures Congress*, Vancouver, BC, Canada, April 24–26, 2008.

Miyamoto HK, Gilani ASJ, Wada A, Ariyaratana C. 2009a. Limit states and failure mechanism of viscous dampers and implications for large earthquakes. *Earthquake Engineering & Structural Dynamics* [accepted].

Miyamoto HK, Gilani ASJ, Wada A, Ariyaratana C. 2009b. Probabilistic collapse performance evaluation of steel moment-frame buildings with viscous dampers. *Earthquake Spectra* (in review).

NEHRP (National Earthquake Hazards Reduction Program). 2009. *FEMA P695: Recommended Methodology for Quantification of Building System Performance and Response Parameters*. Applied Technology Council: Redwood City, CA.

PEER (Pacific Earthquake Engineering Research Center). 2009a. *Next Generation Attenuation of Ground Motions (NGA) Project*. PEER, University of California: Berkeley, CA.

PEER (Pacific Earthquake Engineering Research Center). 2009b. *Open System for Earthquake Engineering Simulation (OpenSees)*. PEER, University of California: Berkeley, CA.

Vamvatsikos D, Cornell CA. 2005. Seismic performance, capacity and reliability of structures as seen through incremental dynamic analysis. *John A. Blume Earthquake Engineering Center report no. TR-151*, Department of Civil and Environmental Engineering, Stanford University, Palo Alto, CA.

Copyright © 2010 John Wiley & Sons, Ltd.

DOI: 10.1002/tal